Available online at www.sciencedirect.com
ScienceDirect
Acta Materialia 59 (2011) 1644–1650
Acta MATERIALIA
www.elsevier.com/locate/actamat

Structural and microstructural analyses of crystalline Er_2O_3 high-k films grown on Si (0 0 1) by laser molecular beam epitaxy

X. Wang [a], Y.L. Zhu [a,*], M. He [b], H.B. Lu [b], X.L. Ma [a]

[a] Shenyang National Laboratory for Materials Science, Institute of Metal Research, Chinese Academy of Sciences, Shenyang 110016, China
[b] Beijing National Laboratory for Condensed Matter Physics, Institute of Physics, Chinese Academy of Sciences, Beijing 100190, China

Received 3 October 2010; received in revised form 1 November 2010; accepted 12 November 2010
Available online 7 December 2010

Abstract

Erbium oxide (Er_2O_3) films are well regarded as being suited for high-k replacement of SiO_2 in endeavors to further miniaturize and enhance the performance of microelectronics. Er_2O_3 films were deposited on Si (0 0 1) substrates by laser molecular beam epitaxy. The structures and microstructures of the films and the interfacial layers were characterized by means of X-ray diffraction (XRD) and transmission electron microscopy (TEM). The results from the XRD and selected area electron diffractions of Er_2O_3 films with thicknesses of 30 and 100 nm indicate that the films are polycrystalline, with dominant (1 1 1) textures of Er_2O_3 {1 1 1} // Si (0 0 1). Amorphous layers dotted with small ordered islands were observed and confirmed to be located at the interfaces between the films and the Si substrates with dark-field image and high-resolution TEM. High-resolution Z-contrast imaging, energy dispersive X-ray spectroscopy and energy-filtered imaging were applied to identify the compositions of the interfacial layers. The salient feature is that the layers consist primarily of Er and O, with a very small amount of Si. This kind of Er–O-based interface layer may play a very important role in the electrical and optical properties of the films.

Keywords: Thin films; High-resolution electron microscopy; Energy-filtered transmission microscopy; Interface; Dielectrics

1. Introduction

The continuing scaling of the dimensions of complementary metal oxide semiconductor devices has prompted extensive research in rare earth metal oxide films as alternative dielectrics for SiO_2 [1–5]. Of the rare earth metal oxide films, Er_2O_3 thin films have attracted much attention recently for their multi-functionality in various fields. Due to the combination of a relatively high dielectric constant (~10–14) [6–9], a wide band gap (7.6 eV), large conduction band offset on Si (3.5 eV) [10], and less interface reaction [11], Er_2O_3 is a promising candidate as a high-k dielectric. In addition, there is increasing interest for its optoelectronic applications. Compared to Er-doped Si-based materials or Er-doped SiO_2, Er_2O_3 films grown on Si have a high concentration of efficient light emitting centers and the advantage of the Er^{3+} ion exhibiting intense photoluminescence [12–14]. Additionally, it can be used as an antireflective and protective coating [15].

Up to now, various kinds of deposition methods have been used to grow Er_2O_3 films, such as electron-beam-gun deposition, molecular beam epitaxy (MBE), magnetron sputtering, reactive RF sputtering, and metal organic chemical vapor deposition [8,9,13,16–18]. Most of these methods are found to produce polycrystalline Er_2O_3 with partial (1 1 1) preferential orientation, except for the films grown by MBE, which have an epitaxial relationship with Si and have two types of (1 1 0) oriented domains. The variance of the microstructures or the stack sequences of the films by different fabrication procedures induce differences in electronic or optical properties of the films. It is generally accepted that a layer of only a few nanometers of low dielectric constant silicon dioxide or metal silicide

* Corresponding author. Tel.: +86 24 83978629; fax: +86 24 23971215.
E-mail address: ylzhu@imr.ac.cn (Y.L. Zhu).

1359-6454/$36.00 © 2010 Acta Materialia Inc. Published by Elsevier Ltd. All rights reserved.
doi:10.1016/j.actamat.2010.11.031

can reduce the capacitance of the stack and significantly degrade the electrical performance of the device [19].

Usually, it is difficult to control the structure and composition of the interface during the film growth process due to the oxidation of Si. In high-k metal oxide films, such as Ta_2O_5, Y_2O_3, Pr_2O_3, HfO_2, and La_2O_3, a layer of amorphous SiO_2 was found to form at the interface between metal oxides and silicon during the deposition or post deposition annealing [1–5]. In the case of Er_2O_3 films, an amorphous SiO_2 interfacial layer also existed, and the interfacial layer was 2–3.5 nm thick depending on the deposition methods [9,20,21]. An $ErSi_2$ layer also formed through the MBE deposition method when the growth conditions were not properly selected [17,18]. However, as mentioned above, it is very important to minimize the formation of SiO_2, silicate, and/or silicides because they degrade the gate stack capacitance through their low-k dielectric constant. In the present work, we report a two-step approach to growing pure {1 1 1} oriented crystalline Er_2O_3 thin films on Si by laser MBE. In contrast with the previous reports, an amorphous Er–O-rich layer dotted with ordered islands was identified at the interface instead the formation of amorphous SiO_2 or $ErSi_2$.

Moreover, the investigations on Er_2O_3/Si systems have been mainly concerned with the electrical and structural properties of the films in the past few years. Few studies have been focused on the microstructure and composition of the Er_2O_3/Si interface in the real space. Although it was previously reported that the structures of Er_2O_3 films on Si were characterized by X-ray diffraction (XRD) and X-ray photoelectron spectroscopy [8,17], some uncertainties, like surface roughness of Si or local chemical distributions at the interface, still exist because these characterization methods only collect averaged information of the samples. Transmission electron microscopy (TEM) with a combination of real space imaging and spectroscopy leads to a more precise and reliable structure analysis, providing a direct interpretation of chemical and microstructural information of the interface. Here we present an elaborate analysis of microstructures and compositions of the films and the interface by taking full advantage of TEM imaging capabilities.

2. Experimental procedure

Er_2O_3 thin films with thicknesses of 30 and 100 nm were deposited on Si (0 0 1) substrates by laser MBE technique. An excimer laser with a wavelength of 308 nm was employed together with in situ reflection high-energy electron diffraction (RHEED) to monitor the crystallization of Er_2O_3. Prior to Er_2O_3 growth, the Si substrates were wet-chemically cleaned and dipped in HF solution to remove the native silicon oxide on the surface, leaving a hydrogen-terminated surface. The Si substrates were then immediately transferred into the chamber. Subsequently the Er_2O_3 films were deposited in a two-step procedure. In the first step, about 2–3 unit cells of Er_2O_3 were deposited under the base pressure of 10^{-5} Pa at room temperature. After that, the substrates were heated to 620 °C and kept at this temperature until sharp streak RHEED patterns were observed. For the second step, the Er_2O_3 films were continuously deposited to the desired thickness under the oxygen pressure of 3×10^{-4} Pa at the temperature of 620 °C. The energy density of the laser at the target was 1 J cm^{-2} and the laser repetition rate was 2 Hz. The deposition rate was about 13 Å min^{-1}.

XRD measurements with θ–2θ scan mode were carried out on a Rigaku D/Max-2500PC diffractometer using Cu Kα X-ray irradiation. TEM specimens for both cross-sectional and plan view observations were prepared by conventional method, i.e., by slicing, grinding, dimpling, and finally ion-milling. A Gatan precision ion polishing system with a liquid-nitrogen-cooled stage was used to prevent the cross-sectional specimens from preferential thinning effects. Plan view specimens were milled only from the substrate side. A Tecnai G^2 F30 transmission electron microscope, equipped with a high-angle-annular-dark-field (HAADF) detector, energy dispersive X-ray spectroscopy (EDS) systems and a post-column Gatan imaging filter, was used for high-resolution TEM, Z-contrast imaging, composition line-scanning analysis and elemental mapping. During the EDS line-scan measurements, a sub-nanometer probe (approximately 0.3 nm in diameter) with a step size of 0.5 nm was used. Elemental mapping analysis based on energy-filtered transmission electron microscopy (EFTEM) imaging was performed using the three-window method.

3. Results

3.1. The crystalline structure and microstructure of Er_2O_3 thin films

The θ–2θ XRD patterns for two Er_2O_3 films with thicknesses of 30 and 100 nm are shown at the top and bottom of Fig. 1, respectively, and show the crystal structure and the orientations with respect to the substrates. Besides the

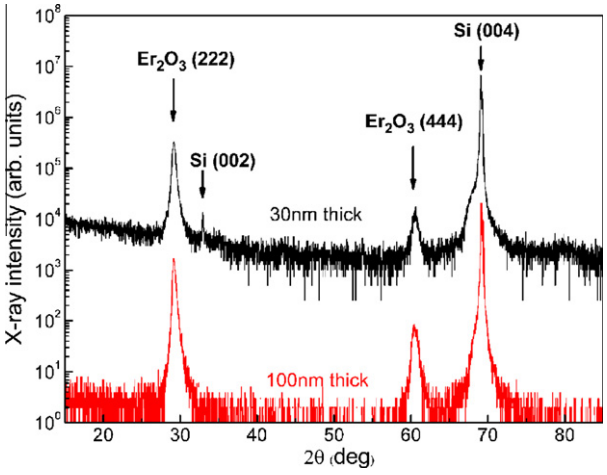

Fig. 1. X-ray diffraction patterns of 30 nm thick and 100 nm thick Er_2O_3 films grown on Si (0 0 1) substrates showing the high degree of texturing of the Er_2O_3 films along {1 1 1}.

strong diffraction peaks from the Si substrates, the only two diffraction peaks which can be distinctly observed are at 29.2° and 60.4°. These two peaks correspond to (1 1 1) and (2 2 2) reflections of the cubic phase Er_2O_3. This indicates that both Er_2O_3 films are crystalline with preferential orientations of Er_2O_3 {1 1 1} // Si (0 0 1), thus suggesting that texturing occurs upon growth. No extra peaks can be found, excluding the formation of any impurities.

To study the structures of the films in detail, both cross-sectional and plan view samples were prepared for TEM observation. Fig. 2a shows a cross-sectional bright-field TEM image of the 30 nm thick Er_2O_3 film. The film has a uniform thickness with a flat surface. Several vertical lines in the film are proposed to be the grain boundaries, which indicate that the Er_2O_3 film may consist of polycrystalline grains. In addition, a uniform interfacial layer can be observed at the interface between the crystalline Er_2O_3 layer and the Si substrate, which is 2–3 nm in thickness. Fig. 2b is a selected area electron diffraction (SAED) pattern corresponding to Fig. 2a. The SAED pattern was recorded in the direction of [1 1 0] of the Si substrate. Besides the strong diffractions from the Si substrate, some weak spots can be identified and indexed as a superposition of $[\bar{1}\,\bar{1}\,0]$, [1 1 0] and [1 2 1] zone axes of cubic Er_2O_3. To clarify the diffraction pattern more clearly, it is necessary to superimpose the calculated diffraction patterns of Er_2O_3 $[\bar{1}\,\bar{1}\,0]$, Er_2O_3 [1 1 0], and Er_2O_3 [1 2 1] in order to simulate the observed one. The simulated results together with Si [1 1 0] zone axes were shown and compared on the right of Fig. 2b. The symbol × stands for the reflections of Si substrate, which should not appear due to the diamond glide plane. The simulated pattern is in good agreement with the experimental one. It is worthy to point out that the polycrystalline Er_2O_3 films grow in such a way that all $(2\bar{2}2)$ planes are parallel to Si (0 0 1) despite having different zone axes, as denoted by the arrowheads in Fig. 2b. The 100 nm thick film was investigated by the same TEM methods and shows the same results. The SAED patterns of both Er_2O_3 films generally show arcs, which are a typical textured polycrystalline characteristic. The cross-sectional BF images in combination with the corresponding diffraction patterns indicate that the Er_2O_3 films grew in the form of totally (1 1 1) oriented polycrystalline grains, which is consistent with the XRD result of Fig. 1.

To get information on grain size and distribution, plan view observations were performed. Fig. 3a–d show typical plan view BF images and corresponding SAED patterns for the films with 30 and 100 nm thickness, respectively. A large number of Er_2O_3 grains were observed in both BF images. The average grain size (30–40 nm) in the 30 nm film (Fig. 3a) is a little smaller than that (40–50 nm) in the 100 nm film (Fig. 3c). For the 30 nm thick film, some grains show Moiré fringe contrast at certain incident conditions, while for the 100 nm thick films no fringe contrast can be observed. The reason for this difference may lie in double diffraction effect, which is directly responsible for the appearance of Moiré fringes, whereas the effect here is influenced by the thicknesses of the two crystal layers. To facilitate the determination of the structures of the films from the plan view direction, the SAED patterns were recorded with the incident electron beam parallel to the texture axis (i.e. Er_2O_3 $[1\,\bar{1}\,1]$ or Si [0 0 1]) by tilting, and under this condition they display ring patterns as shown in Fig. 3b and d. The inter-planar

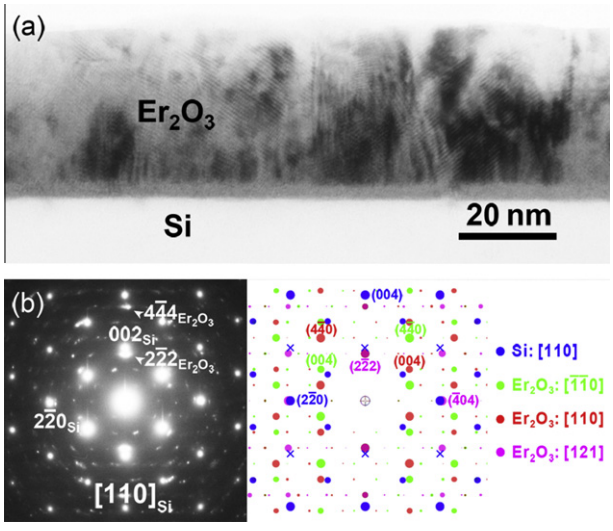

Fig. 2. (a) Low-magnification cross-sectional bright-field TEM image showing the morphology of the 30 nm thick Er_2O_3 film grown on Si (0 0 1). The film is polycrystalline and an interfacial layer lies at the film/substrate interface and (b) corresponding SAED pattern taken from the area covering both the film and the Si substrate. The right is the simulated pattern superposed by patterns of Er_2O_3 $[\bar{1}\,\bar{1}\,0]$, Er_2O_3 [1 1 0], Er_2O_3 [1 2 1] and Si [1 1 0] with all Er_2O_3 $(2\bar{2}2)$ planes parallel to the Si (0 0 1).

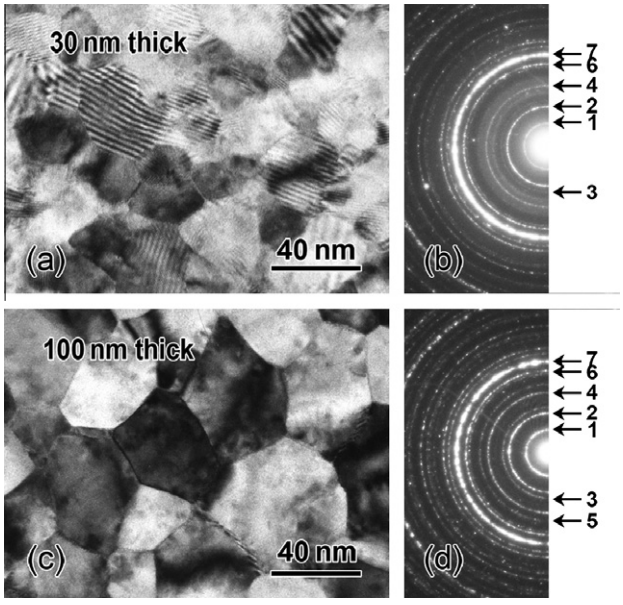

Fig. 3. Plan view bright-field TEM image showing nano-sized grains in the Er_2O_3 films and the corresponding SAED patterns recorded with the incident electron beam parallel to the texture axis: (a and b) for 30 nm thick film, (c and d) for 100 nm thick film. The numbered diffractions were indexed as seen in Table 1.

d-spacings of the rings calculated from Fig. 3b and d were summarized and compared to the bulk one (JCPDS No. 08-0050) as given in Table 1. From Table 1, it is noted that the strong reflections reported in JCPDS, such as (2 2 2) and (4 0 0) of Er_2O_3, were missing in Fig 3b and d. In addition, all present reflections can be indexed to the $[1\,\bar{1}\,1]$ zone axis of Er_2O_3, although some of the kinematically forbidden reflections such as {1 1 0} and {3 3 0} were also present due to dynamical effects. The results from plan view observations give further evidence of the polycrystalline structure of the films textured with Er_2O_3 (1 1 1), in agreement with the XRD and the cross-sectional results presented above.

3.2. The interface of Er_2O_3/Si

To explore the structural nature of the interfacial layer, dark-field (DF) TEM was used. Fig. 4a is a low-magnification cross-sectional DF image of the 30 nm thick Er_2O_3 film using Er_2O_3 $\mathbf{g} = (2\bar{2}2)$. Fig. 4b shows the reflections. Under this condition, only the film is diffracted and appears bright. Besides the bright contrast areas, some diffuse lines showing dark contrast can be observed. These lines start from the bottom of the crystalline Er_2O_3 layer and in some cases penetrate the whole film, and are believed to be the grain boundaries. In addition to the crystalline Er_2O_3 layer, some weak bright contrast comes from the area between the crystalline Er_2O_3 and the Si substrate, indicating a certain degree of crystallization in the interfacial layer.

Cross-sectional high-resolution TEM (HRTEM) images of the two films show the details about the interfacial layers as seen in Fig. 5. Crystalline Er_2O_3, the interfacial layer and the Si substrate are clearly visible for both films. The interfacial layers are amorphous with some small ordered islands, consistent with the DF results. The thicknesses of the interfacial layers are 2.2 nm and 2.6 nm for the 30 and 100 nm thick films, respectively. The slight difference is possibly due to the film thickness effect.

Table 1
Indexing of the rings in diffraction patterns from the plan view in Fig. 3b and d. The measured inter-planar *d*-spacings and the calculated ones based on bulk parameters are compared.

No. in Fig. 3	*d* (Å)			Indices of the plane
	30 nm thick film	100 nm thick film	Bulk[a]	
1	7.35	7.43	7.46	{1 1 0}[b]
2	4.30	4.30	4.31	{2 1 1}
3	3.72	3.72	3.73	{2 2 0}
4	2.81	2.82	2.82	{3 2 1}
5		2.50	2.49	{3 3 0}[b]
6	2.06	2.07	2.07	{4 3 1}
7	1.86	1.87	1.86	{4 4 0}

[a] Calculated based on JCPDS (No. 08-0050).
[b] The kinematically forbidden reflections which were present due to dynamical scattering events.

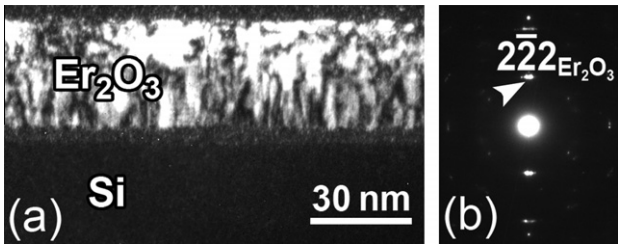

Fig. 4. (a) Cross-sectional dark-field image of the 30 nm thick Er_2O_3 film showing the amorphous interfacial layer with a certain degree of crystallization; (b) the $\mathbf{g}_{2\text{–}22}$ vector of Er_2O_3 used to obtain the dark-field image.

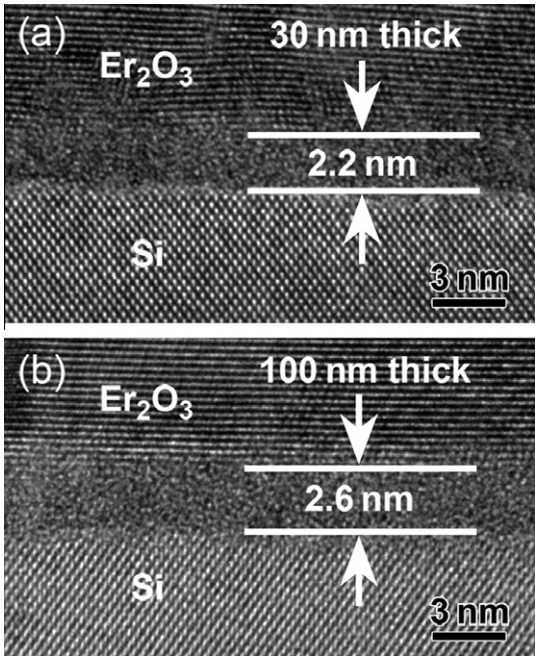

Fig. 5. Cross-sectional HRTEM images of the film/substrate interface showing the amorphous interfacial layer with small ordered islands: (a) for 30 nm thick film; (b) for 100 nm thick film.

Fig. 6 shows a cross-sectional high-resolution HAADF image of the 30 nm thick Er_2O_3 film on Si substrate. In the image, only incoherent scattered electrons at high angles are collected during the imaging and the contrast can simply be interpreted by the atomic number differences, namely, Z-contrast. It is evident that the uniform interfacial layer is formed between the lattice of the crystalline Er_2O_3 and that of the Si substrate. The amorphous interfacial layer displays a much brighter contrast than Si and a little darker contrast than crystalline Er_2O_3, indicating that the concentration of the heavy element Er is high. Some interdiffusion zone (of Si, diffusing into the amorphous Er–O (Si) layer) is visible, for there is a transition from Si substrate to the first amorphous layer as seen in Fig. 6.

To clarify the compositional variations of the films at the interface, a sub-nanometer chemical analysis with EDS in TEM was performed. Fig. 7a is a low magnification HAADF image, in which the amorphous interfacial layer is

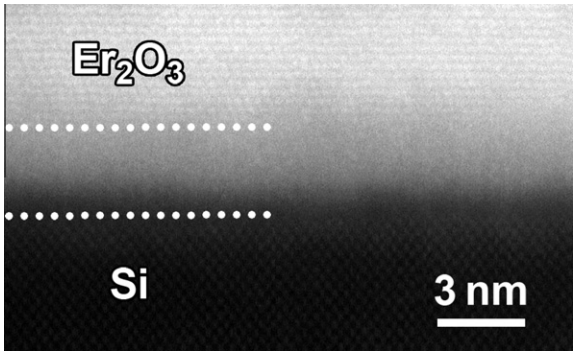

Fig. 6. Cross-sectional high-resolution HAADF image of the Er_2O_3 film on Si substrate. The interfacial layer showing bright contrast implies the layer is rich in heavy elements.

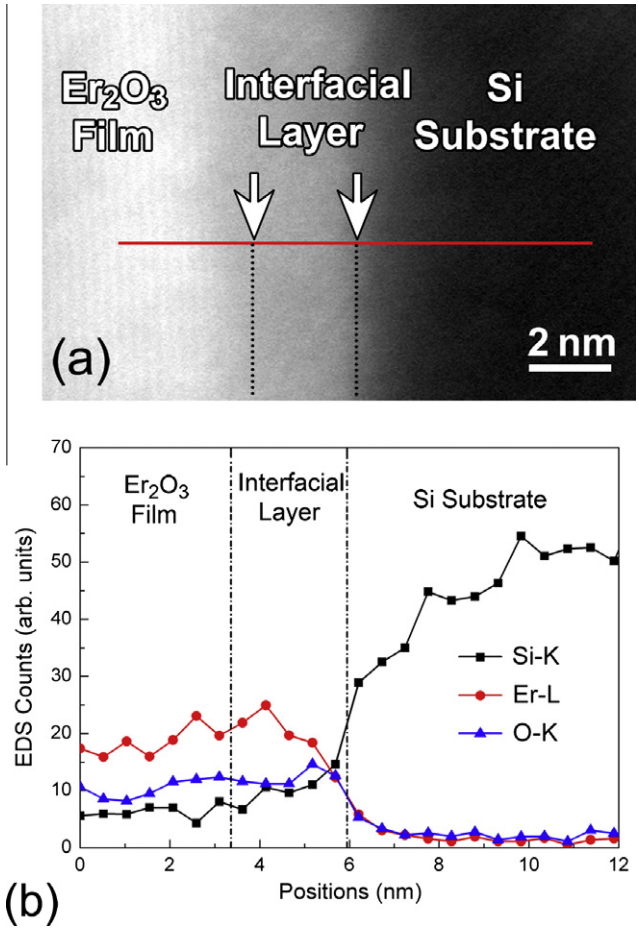

Fig. 7. (a) Cross-sectional HAADF image showing the crystalline Er_2O_3 film, the interfacial layer, and the Si substrate; (b) EDS line-scan profiles scanned along the red line in (a). The interfacial layer is mainly composed of Er and O. (For interpretation of the references to color in this figure legend, the reader is referred to the web version of this article.)

marked by downward arrows. The EDS line-scan profile shown in Fig. 7b was carried out along the route of the red line in Fig. 7a. The plots at the left side result from the scanning of the crystalline Er_2O_3 film and the right side shows the results of the Si substrate. When the line scan goes from the Si substrate to the interfacial layer, the composition changes dramatically. Within the band, the counts of Er and O increase distinctly, while the count of Si decreases rapidly, implying that there is much less Si in the interfacial layer than in the substrate. As a result, the amorphous interfacial layer is mainly composed of Er and O, with only a small amount of Si found primarily in the area directly adjacent to the interface.

Elemental mapping with an EFTEM based on inelastic electron scattering has the advantages of high efficiency and high energy resolution at nanometer length scales, which is appropriate for investigating the elemental distribution of the film and the interface. Fig. 8a is a cross-sectional BF image of the 30 nm thick Er_2O_3 film filtered with zero loss peak (ZLP). The interface between the film and the Si substrate is sharp and flat. The interface layer shows bright contrast. The corresponding energy-filtered erbium map was recorded and is shown in Fig. 8b. It clearly demonstrates that the amorphous layer contains a little less of the element Er than the main crystalline Er_2O_3 layer does, as denoted by white hollow arrow. In addition, the oxygen map in Fig. 8c indicates a little less element O in the amorphous interfacial layer than that in the main crystalline layer as well. Furthermore, the silicon map was also recorded as seen in Fig. 8d. It displays subtle contrast at the amorphous interfacial layer, indicating that a small amount of the element Si has penetrated from the substrate into the interfacial layer with some local segregation. On the whole, the chemical composition of the amorphous interfacial layer has been identified to be high concentrations of Er and O, and a low concentration of Si.

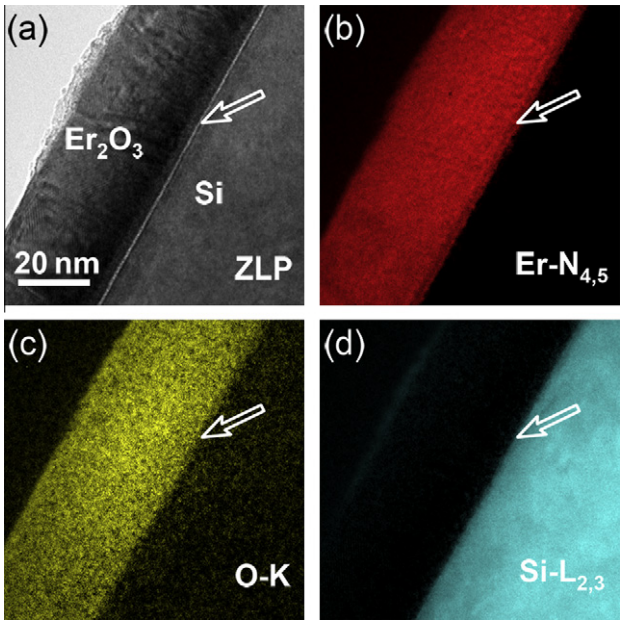

Fig. 8. EFTEM images of Er_2O_3/Si layer structure demonstrating composition variations of the interfacial layer. (a) BF image filtered with zero loss peak; (b) Er–$N_{4,5}$ elemental map; (c) O–K elemental map; (d) Si–$L_{2,3}$ elemental map. The film/substrate interface was marked by white hollow arrows.

4. Discussion

The structural character of our Er_2O_3 films grown on Si (0 0 1) substrates was identified to be {1 1 1} orientation polycrystalline with a 2–3 nm thick interfacial layer at the film/substrate interface. The interfacial layer is amorphous with a certain degree of crystallization, and is mainly composed of Er and O, with a low concentration of Si. These characteristics are the direct result of our two-step film growth approach, and may be found to improve the electrical or optical properties of the films.

4.1. Formation of crystalline Er_2O_3 films with {1 1 1} orientation

The main reason for the formation of the Er_2O_3 films with {1 1 1} preferential orientation is believed to be the low surface energy of {1 1 1} planes in cubic phase Er_2O_3. The cubic Er_2O_3 phase has a bixbyite Mn_2O_3 structure with the space group symmetry $Ia\bar{3}$. In general, the surface energy is a result of the disruption of bonds that occur when a surface is created. For the structure of Er_2O_3, the {1 1 1} plane is the close-packed plane. The number of disrupting bonds per unit area is the least when the {1 1 1} surface is created. Excluding the contributions of surface relaxation and electrical dipole, the {1 1 1} surface of Er_2O_3 has the lowest surface energy. In fact, a unit cell of Er_2O_3 consists of eight unit cells of an incomplete CaF_2 structure with one quarter of the oxygen sites vacant. Consulting the first principle studies of CeO_2 which has a CaF_2 structure, the (1 1 1) surface has lower energy than {1 0 0} and {1 1 0} [22,23]. Therefore, the low surface energy is the driving force for the growth of the {1 1 1} oriented Er_2O_3 films.

It was previously reported that the epitaxial growth of Er_2O_3 films on Si (0 0 1) by molecular beam epitaxy is with Er_2O_3 (1 1 0) // Si (0 0 1), Er_2O_3 [0 0 1] // Si [1 1 0] or Er_2O_3 [1 1 0] // Si [1 1 0] [7,17]. However, their crystalline Er_2O_3 had two variants of orientations with respect to Si (0 0 1), which favors the formation of a potentially harmful microstructure, and there were ripples at the domain boundaries. In contrast with the epitaxial films, our Er_2O_3 films grown on Si (0 0 1) substrates are polycrystalline with full (1 1 1) texturing out-of-plane and with random directions in-plane. During the film growth, the constraint from the Si substrate, like the interface bonding or lattice misfit strain, did not work. Only the minimization of the surface energy controlled the film growth to create this film orientation. With a low surface energy plane {1 1 1} as the growth plane, the films may exhibit a flatter surface, which matches well with the results from Losurdo et al., who studied erbium oxides prepared by metal organic chemical vapor deposition [9].

4.2. Formation mechanism of the amorphous interfacial layer and its potential effect on electrical and optical properties of films

One important issue raising concerns about the suitability of Er_2O_3 for high-k gate applications is the formation of an amorphous layer at the interface. This has been mainly attributed to SiO_2, silicides, and/or silicates undergrowth due to either the diffusion of both Si and oxygen atoms or the reaction between Si and Er_2O_3 oxide during deposition. On the one hand, Si reacts easily with O. Also, the diffusion reaction is thermally activated. Although the oxygen pressure is purposely kept low during our growth process, the oxygen diffusivity will be enhanced and oxygen atoms will diffuse to the Si substrate during the film growth process. As a result, the oxidation of Si is, to some extent, unavoidable. On the other hand, despite the good thermodynamic stability of Er_2O_3 predicted by Hubbard and Schlom [24], the reaction between Si and Er_2O_3 films is possible depending on the deposition methods and deposition parameters. However, it is very important to minimize the formation of SiO_2, silicate and/or silicides interfacial layers in order to maximize the gate stack capacitance. In the present study, a thin Er_2O_3 layer with a 2–3 unit cell thickness was initially grown at room temperature and low oxygen pressure on clean Si substrate. This layer will act to reduce the diffusion of Si from the substrate to the films and suppress the formation of erbium silicide interfacial phases during the growth of the films. Therefore, an amorphous layer, primarily of Er and O content, is formed on top of the Si substrate as evidenced by our structural and compositional results. The substrates were then heated to a high, constant temperature (620 °C) until the desired crystal characteristic was detected with the RHEED monitoring system. As a result, the amorphous layer was, to some extent, crystallized at high temperature. During this heating process a small amount of Si atoms might diffuse from the substrate to the amorphous layer and form a concentration gradient in the amorphous layer.

It was reported that the surface roughness of the films grown on a clean Si substrate surface was larger than that of the films grown on an oxidized Si substrate surface, which might be due to the poor crystallinity or the Er silicide formation at the interface [17,25]. In our films, the amorphous Er–O–Si layers grown at room temperature depressed the formation of silicon dioxide and erbium silicide at the film/substrate interfaces and improved the surface roughness. Moreover, as stated previously, the Er-containing interfacial layer shows a significantly higher refractive index than that of SiO_2 and the erbium oxides demonstrate higher currents and lower breakdown fields than for SiO_2 [9]. It is inferred that high concentrations of Er and O in the present interfacial layers may help improve the performances in electrical and optical applications via increasing the capacitance or the light emission efficiency.

5. Conclusions

A two-step approach was applied to our Er_2O_3 film growth on Si (0 0 1) substrates by laser MBE. By an elaborate transmission electron microscopy analysis, we find that the Er_2O_3 films consist of {1 1 1} oriented

nanocrystalline grains. This orientation follows from surface energy minimization. At the interface between the crystalline Er_2O_3 films and Si substrates, an interfacial layer forms. The layer may primarily form at the initial stage of the film growth when room temperature and low pressure conditions were used. The layer is amorphous and acquires a certain degree of crystallization during the heating after the first step, which was demonstrated by dark-field and high-resolution TEM. According to the results of the energy dispersive X-ray spectroscopy line-scan and the elemental mapping, the layer contains high concentrations of Er and O, and low concentrations of Si. The structural and compositional characteristics of the Er_2O_3 films and the interface layer exhibit a strong correlation with the film growth procedure, and this unique structure may improve the electrical and optical properties of the Er_2O_3 films.

Acknowledgements

This work was supported by the National Basic Research Program of China (2009CB623705), and the National Natural Science Foundation of China (No. 50871115).

References

[1] Alers GB, Werder DJ, Chabal Y, Lu HC, Gusev EP, Garfunkel E, et al. Appl Phys Lett 1998;73:1517.
[2] Dimoulas A, Vellianitis G, Travlos A, Ioannou-Sougleridis V, Nassiopoulou AG. J Appl Phys 2002;92:426.
[3] Lo Nigro R, Toro RG, Malandrino G, Raineri V, Fragala IL. Adv Mater 2003;15:1071.
[4] Baik HS, Kim M, Park GS, Song SA, Varela M, Franceschetti A, et al. Appl Phys Lett 2004;85:672.
[5] Inamoto S, Yamasaki J, Okunishi E, Kakushima K, Iwai H, Tanaka N. J Appl Phys 2010;107:124510.
[6] Mikhelashvili V, Eisenstein G, Edelmann F. Appl Phys Lett 2002;80:2156.
[7] Chen S, Zhu YY, Xu R, Wu YQ, Yang XJ, Fan YL, et al. Appl Phys Lett 2006;88:222902.
[8] Pan TM, Chen CL, Yeh WW, Hou SJ. Appl Phys Lett 2006;89:222912.
[9] Losurdo M, Giangregorio MM, Bruno G, Yang D, Irene EA, Suvorova AA, et al. Appl Phys Lett 2007;91:091914.
[10] Zhu YY, Chen S, Xu R, Fang ZB, Zhao JF, Fan YL, et al. Appl Phys Lett 2006;88:162909.
[11] Ono H, Katsumata T. Appl Phys Lett 2001;78:1832.
[12] Kasuya A, Suezawa M. Appl Phys Lett 1997;71:2728.
[13] Miritello M, Lo Savio R, Piro AM, Franzo G, Priolo F, Iacona F, et al. J Appl Phys 2006;100:013502.
[14] Michael CP, Yuen HB, Sabnis VA, Johnson TJ, Sewell R, Smith R, et al. Opt Express 2008;16:19649.
[15] Losurdo M, Giangregorio MM, Capezzuto P, Bruno G, Toro RG, Malandrino G, et al. Adv Funct Mater 2007;17:3607.
[16] Mikhelashvili V, Eisenstein G, Edelmann F. J Appl Phys 2001;90:5447.
[17] Xu R, Zhu YY, Chen S, Xue F, Fan YL, Yang XJ, et al. J Cryst Growth 2005;277:496.
[18] Smith RS, Sewell RH, Clark A, Atanackovic P. J Cryst Growth 2009;311:2199.
[19] Robertson J. Rep Prog Phys 2006;69:327.
[20] Mikhelashvili V, Eisenstein G, Edelman F, Brener R, Zakharov N, Werner P. J Appl Phys 2004;95:613.
[21] Chen S, Zhu YY, Wu R, Wu YQ, Fan YL, Jiang ZM. J Appl Phys 2007;101:064106.
[22] Skorodumova NV, Baudin M, Hermansson K. Phys Rev B 2004;69:075401.
[23] Nolan M, Grigoleit S, Sayle DC, Parker SC, Watson GW. Surf Sci 2005;576:217.
[24] Hubbard KJ, Schlom DG. J Mater Res 1996;11:2757.
[25] Zhu YY, Xu R, Chen S, Fang ZB, Xue F, Fan YL, et al. Thin Solid Films 2006;508:86.